NUMERICAL ANALYSIS OF FREE VIBRATIONS AND WAVE PROPAGATION OF ELASTIC MEDIA BY THE GFEM

Oscar Alfredo Garcia de Suarez, oagsuarez@ucs.br
Departamento de Engenharia Mecânica, Universidade de Caxias do Sul, Rua Francisco Getúlio Vargas, 1130, Caxias do Sul, RS, 95070-560.

Rodrigo Rossi, rrossi@ufrgs.br
Departamento de Engenharia Mecânica, Universidade Federal do Rio Grande do Sul, Departamento de Engenharia Mecânica, Rua Sarmento Leite, 425, Porto Alegre, RS, 90046-902.

Paulo Roberto Linzmaier, prlinzma@ucs.br
Departamento de Engenharia Mecânica, Universidade de Caxias do Sul, Rua Francisco Getúlio Vargas, 1130, Caxias do Sul, RS, 95070-560.

Abstract. *One of the limitations of the Finite Element Method is the lack of precision in the estimation of the high-frequencies eigenmodes. In general, considering a frequency range, the eigenmodes obtained by the Finite Element Method represent a small percentage of the total number of eigenmodes. This problem is even worse when high-order finite elements with low regularity are employed in the numerical analysis. When excited by impulsive forces, the precision of the mechanical wave propagation in elastic solid media depends on the precision that one can represent the eigenmodes. In this sense, the larger the number of modes that can be represented more precisely, the more accurate representation of the propagating wave. In this work we present a Generalized Finite Element Method (GFEM) that is used to solve the free vibration and wave propagation problem in elastic solid media. The proposed GFEM generates high regularity approximation spaces. More specifically, we explore the p version of the method in which the Partition of Unity, which are constructed based on rational polynomial weight functions, are enriched by monomials of order p. The dynamic solution is obtained based on the implicit Newmark method and the modal superposition. Cases of study are carried out considering linear elastic rods and axisymmetric plates and shells submitted to impulsive forces.*

Keywords*: Natural frequencies, wave propagation, GFEM.*

1. INTRODUCTION

The problem of obtaining high natural frequency modes precisely by using numerical methods is still an open research topic that includes several proposals. The Finite Element Method (FEM), which is currently a consolidated method, has some limitations in accurately obtaining natural frequencies. Several works in the literature deal with the correct determination of eigenmodes in elliptical problems. An *a priori* error estimator for the so-called *h* version of the FEM, see Hughes (1987) and more recently Givoli (2007), is available. This error estimator is

$$e_n = \left|\lambda_n^h - \lambda_n\right| \le Ch^{2(p-s)}\lambda_n^{(p+1)/(s+1)}, \tag{1}$$

where λ_n is the exact n^{th} eigenvalue, λ_n^h is the FEM approximation eigenvalue, h is a mesh parameter, i.e., the size of the largest element in the mesh, C is a constant independent of h and λ_n, p is the polynomial degree of the FEM approximation space and s is the regularity of the FEM approximation space (C^s).

In the work presented by Cottrell *et al.* (2007a, 2007b), the outstanding superiority of the so-called *k*-method, as compared to the FEM results, for finding the eigenmodes of elliptic eigenvalue problems was presented. The results presented by this work showed an absence of acoustic and optical branches.

In this work, we employ a Generalized Finite Element Method (GFEM) equipped with an approximation space that has high order and regularity. The Partition of Unity (PU) generated in this work is obtained by rational polynomial weight functions and presents regularity $C_0^k(\Sigma), k = 0, 2, 4$. In addition, the PUs are homogenously enriched by a set of monomials of p. Some examples are presented to attest the use of the proposed methodology in addressing of free vibrations and wave propagation problems in linear elastic media.

2. ENRICHED GFEM APPROXIMATION SPACE

The GFEM is derived from the methodologies that construct the approximation space based on the PU concept; see Melenk and Babuska (1996) and Oden et al. (1996). The enrichment procedure used in this work consists

in the multiplication of a shape functions, which is based on a rational polynomial weight function, defined on a nodal position of the element of the integration mesh, by a set of monomials of a given order *p*. The nodes to be enriched can be selectively selected, by means of an error estimator and *p*-refinement, or simply homogeneously selected. In the case of curved domains, which is one of the purposes of analysis of this work, the enriched functions are defined on a parametric domain Σ and then mapped to the physical domain by a vector mapping function $\mathbf{X}(s)$, where *s* is the arc-length, see Fig. 1. For a detailed description see Garcia and Proença (2007).

The enriched approximation space is equipped with all the possible linear combinations of a finite dimension space generated by the product of PU functions φ_α by a set of functions Q_α^p, which is the Local Approximation Space. Here α is the node or particle number. Some important definitions are presented in order to aid the presentation of the global approximation space. The global approximation space of order *p* is defined as

$$\Im_N^p = span\left[\left\{\varphi_\alpha Q_\alpha^p\right\}_{\alpha=1}^N\right] \tag{2}$$

Figure 1 shows an example of a local space generated by a PU formed by linear functions. In this example $\rho_2 = \left\{1, \overline{s}, \overline{s}^2\right\}$ and the local approximation space is given by $Q_\alpha^2 = span\left[\left\{1, \overline{s}, \overline{s}^2\right\}\right]$. Figures. 1(b) and 1(c) show the functions ψ_2^α and ψ_3^α that are the basis of the enriched approximation space. Figures 1(d) and 1(e) show the mapping $\mathbf{X}: \Sigma \to \Omega$, which maps the enriched PU approximation space from the parameterized domain to the physical domain, see Garcia and Proença (2007).

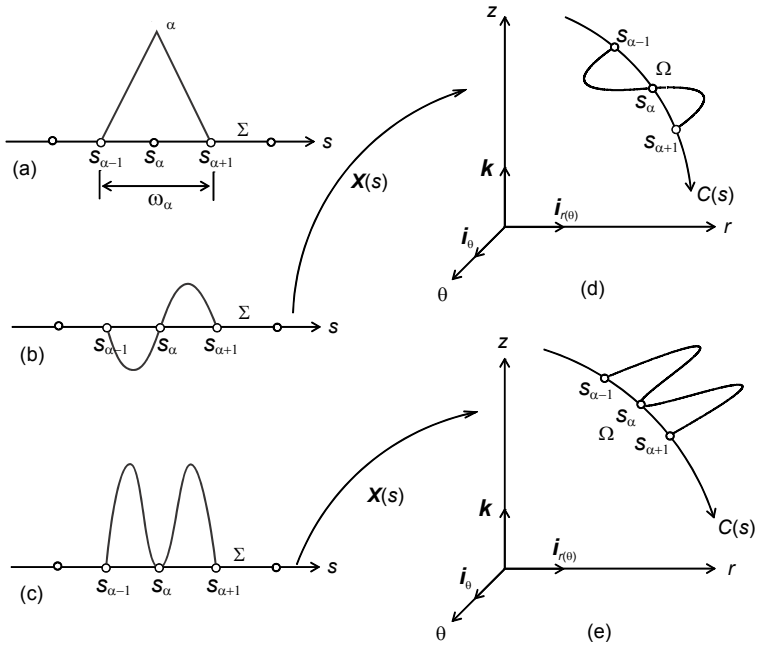

Figure 1 - Examples of mapping from the parametric to physical domain. (a) Linear PU; (b) $\psi_2^\alpha = \overline{s}\varphi_\alpha$; (c) $\psi_3^\alpha = \overline{s}^2\varphi_\alpha$; (d) Mapping function ψ_2^α in the physical domain; (e) Mapping function ψ_3^α in the physical domain.

2.1. PUs constructed based on rational polynomial weight function

The PU functions presented in this work are Shepard functions that are constructed based on rational polynomials weight function. In a general manner, the weight functions are defined on R as follows: Let the weight functions $W_\alpha : \mathsf{R} \to \mathsf{R}$ be such that $W_\alpha \in C_0^k, k \geq 0$, with the following features:

i. $W_\alpha\left(\overline{s}\right) \geq 0, \forall \overline{s} \in \Sigma$,

ii. $W_\alpha\left(\overline{s}\right) = W_\alpha\left(s - s_\alpha\right), W_\alpha \in C_0^k, k \geq 0$ and

iii. $\forall \overline{s} \in \overline{\Sigma} \to card\left\{\alpha \mid \overline{s} \in \omega_\alpha\right\} \leq M \in \mathsf{N}^+$.

where $\bar{s}$ is the coordinate in relation to the node α. The proposed family of weight functions defined on the global parametric domain Σ is

$$W_\alpha(s)=\begin{cases}0 & if\ s<s_\alpha-{}^{h_\alpha}\!/_2\\ \left[1-\left(\dfrac{s-s_\alpha}{{}^{h_\alpha}\!/_2}\right)^m\right]^n & if\ s_\alpha-{}^{h_\alpha}\!/_2\le s\le s_\alpha+{}^{h_\alpha}\!/_2\ for\ n\ge 1, m=2,4,\ldots\\ 0 & if\ s>s_\alpha+{}^{h_\alpha}\!/_2\end{cases} \tag{3}$$

where $h_\alpha = size(\omega_\alpha)$. Here we assume, for sake of simplicity, that the weight function is centered with relation to ω_α. The proposal presented in this work considers weight functions $W_1(\xi)$ and $W_2(\xi)$, which are defined on the parametric domain of the element ξ. In this case M = 2, i.e., there are a maximum of two weight functions covering each point of the domain. The features of the proposed weight functions can be summarized as follows:

i. $W_\beta(\xi)\in C_0^k, k=0,2,4\ldots,\beta=1,2$ and

ii. $W_\beta(\xi)\ge 0\,\forall\,\xi\in\omega_e$.

Therefore, the Sheppard shape function associated with the node β is

$$\varphi_\beta=\frac{W_\beta(\xi)}{\sum_{\gamma=1}^{2}W_\gamma(\xi)}. \tag{4}$$

Thus, the weight function family proposed in this paper is

$$W_\beta(\xi)=\left[1-\left(\frac{1\pm\xi}{2}\right)^m\right]^n, n\ge 1, m=0,2,4,\ldots,\beta=1,2. \tag{5}$$

After a straightforward analysis of the weight functions in Eq.(3) we reach to the following regularity condition: n odd $\rightarrow W_\alpha(s)\in C^{n-1}$ and n even $\rightarrow W_\alpha(s)\in C^n$.

3. EXAMPLES

3.1. Eigenvalues of a clamped rod

To demonstrate the influence of the approximation space regularity order in the capture of the natural frequencies analysis of a simple problem is carried out. The problem is a rod clamped at one end and submitted to a condition ${}^{du}\!/_{dx}=0$ at the other end. Figure 2 show the model problem and also the material properties.

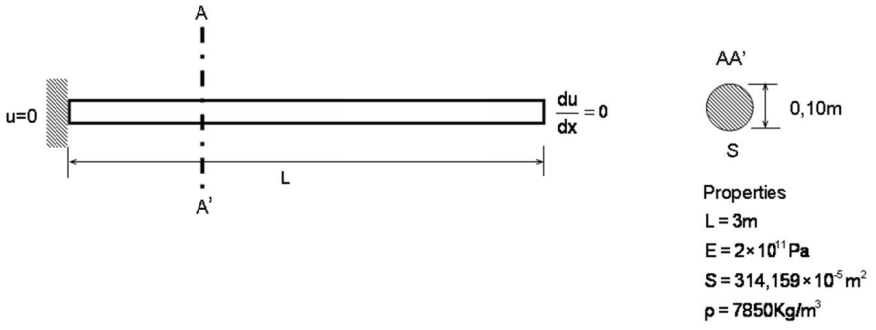

Figure 2. Rod model problem.

The elliptical eigenvalue problem of the model depicted in Fig. 1 can be stated as: Determine the pairs $(\omega_n, u_n(x))$, where $u_n(x)\neq 0$ for any value of $n\in N^*$ that satisfies

$$\frac{d^2u(x)}{dx^2}+\omega^2\frac{\rho}{E}u(x)=0,\ \ \forall x\in(0,L);\quad u(x)=0,\ \ x=0\qquad\text{and}\qquad\frac{du(x)}{dx}=0,\quad x=L \tag{6}$$

The solution of Eq. (6) is given by an infinite set of countable pairs $(\omega_n,u_n(x)),\ n=1,2,...,\infty$ where $0<\omega_1^2<\omega_2^2<,....,<\omega_{i-1}^2<\omega_i^2<\omega_{i+1}^2<,...$ with

$$\omega_n=\frac{j\pi}{2L\sqrt{\rho/E}},\quad j=1,3,5,.....,2n-1;\quad n=1,2,3,...,\infty \tag{7}$$

and

$$u_n(x)=Csen\left(\sqrt{\rho/E}\,\omega_n x\right). \tag{8}$$

The weak for of the problem can be enounced as: Find $\tilde{u}\in Kin$ such that

$$-\int_0^L E\frac{d\tilde{u}}{dx}\frac{dv}{dx}dx+\omega^2\int_0^L\rho\tilde{u}vdx=0,\quad\forall v\in Var\ . \tag{9}$$

where

$$Kin=\left\{\tilde{u}\in H^1(\Sigma)/\tilde{u}=\overline{u},x=0\right\}\ \text{ and }\ Var=\left\{v\in H^1(\Sigma)/v=0,x=0\right\}. \tag{10}$$

The discretized GFEM formulation is given by

$$\int_0^L\mathbf{B}^TE\mathbf{B}dx-\omega^2\int_0^L\rho\mathbf{N}^T\mathbf{N}dx=0\,, \tag{11}$$

in which

$$\mathbf{N}=\left[\psi_1^1\ \ \psi_2^1\ \ \psi_3^1\ \ \cdots\ \ \psi_i^\alpha\ \ \cdots\ \ \psi_p^n\right];\ \mathbf{B}=\left[\psi_{1,x}^1\ \ \psi_{2,x}^1\ \ \psi_{3,x}^1\ \ \cdots\ \ \psi_{i,x}^\alpha\ \ \cdots\ \ \psi_{p,x}^n\right],\ \alpha=1,...,n;\ i=1,...,p. \tag{12}$$

In Eq. (12) ψ_i^α is the global shape function of order *i* associated with the node α.

Figures 3(a) and 3(b) shows the results achieved by the solution of the eigenvalue problem considering two different approximation spaces. The results presented in these figures are shown in terms of the normalized values of the natural frequencies *versus* the normalized number of nodes used in the analysis. In these figures w_h is the approximated result while w is the analytical result. Fig. 3(a) presents the results achieved using the MEF, in which 50 elements were used, where the order *p* of the approximation was augmented accordingly to follow order: linear, quadratic, cubic and quartic. On the other hand, Fig. 3(b) shows the results obtained using the proposed approximation space keeping the same discretization but the enrichment of $p=\{1,2,3,4\}$.

The results presented in Fig. 3(a) were achieved based on C_0^0 MEF. For linear approximation the result is smooth but has low precision. However, when the order *p* is augmented (quadratic, cubic and quartic) there are severe jumps in the numerical solution. Although the procedure presents good precision in the first part of the analysis, jumps in the solution are presented denoting the appearance of the acoustic and optic branches in the spectrum. The jumps are followed by a lost in the numerical solution precision. On the other hand, when the proposed enriched approximation

space is used, Fig. 3(b), we visibly notice the influence of the regularity order in the numerical solution, showing that when the regularity order is augmented an improved solution is obtained.

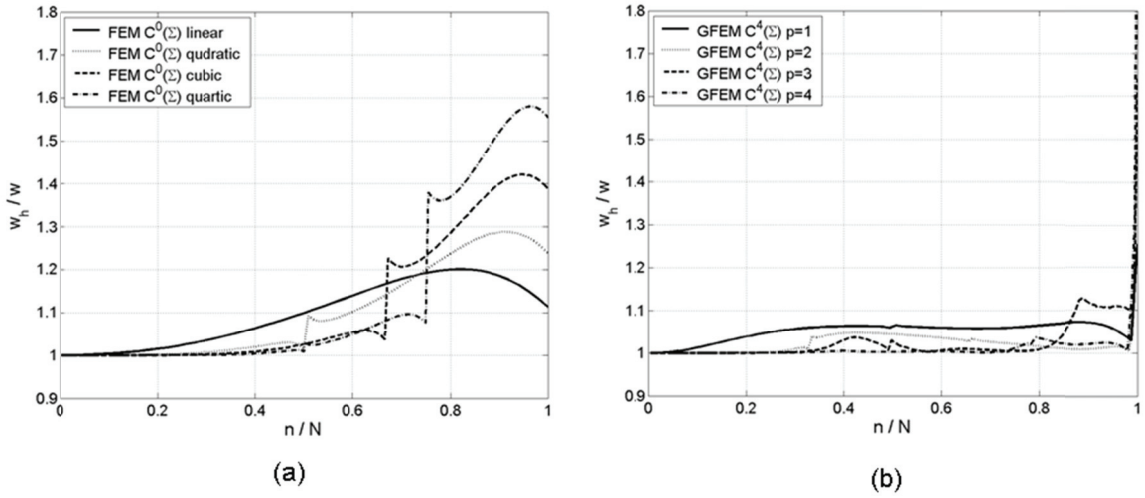

Figure 3 – Normalized natural frequencies values for the model problem. (a) Results for the *p*-FEM version; (b) Results for the enriched space proposed in this work.

3.2. Wave propagation in a rod

The phenomenon of wave propagation in a rod is studied based on the evaluation of the wave front in the displacement field. The problem model is depicted in Fig. 4.

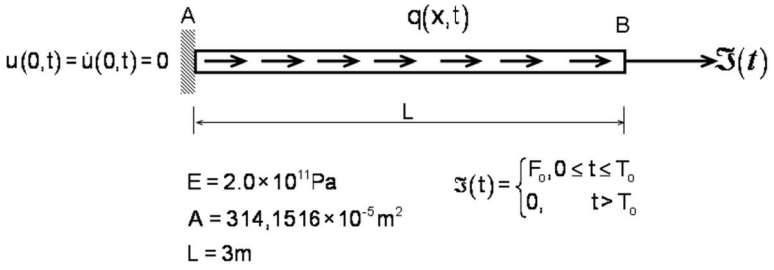

Figure 4 – Rod model problem with natural boundary conditions dependent on time.

The hyperbolic wave propagation model in one-dimensional context is given by the following IBVP:

$$\begin{aligned}
&\frac{\partial^2 \boldsymbol{u}(x,t)}{\partial x^2} + \frac{q(x,t)}{EA} = \frac{1}{c^2}\frac{\partial^2 \boldsymbol{u}}{\partial t^2}, \quad \forall x \in (0,L)\times(0,T) \\
&EA\frac{\partial \boldsymbol{u}}{\partial x} = \Im(t), \quad x = L; \quad \boldsymbol{u}(x,t) = 0, \quad x = 0, \quad t \in [0,T] \\
&\boldsymbol{u}(x,0) = 0, \forall x \in (0,L); \quad \dot{\boldsymbol{u}}(x,0) = 0, \forall x \in (0,L)
\end{aligned} \tag{13}$$

In Eq. (13) $\Im(t)$ is the indicatory function

$$\Im(t) = \begin{cases} F_o, & 0 \le t \le T_o \\ 0, & t > T_o \end{cases}. \tag{14}$$

In the IBVP defined by Eq. (13), $\boldsymbol{u}(\boldsymbol{x},t)$ is the bar axial displacement, *A, E, c* and $q(\boldsymbol{x},t)$ are respectively, the cross sectional area, the Young Modulus, the wave velocity and the distributed load.

The analytical solution of the problem defined by Eq. (13) is given by Eq (15) for a time interval greater than T_o, which is the time interval of the external load imposition. The Eq (15) is obtained based on a zero distributed load, see Clough & Penzien (2003).

$$\boldsymbol{u}(x,t)=\sum_{j=1}^{\infty}\left(\sin\left(k_j x\right)\right)\frac{2F_O\sin\left(k_j L\right)}{\mu\omega_j^2 L}\left[\cos\left(\omega_j\left(t-T_o\right)\right)-\cos\left(\omega_j t\right)\right],\quad \forall t>T_O \tag{15}$$

In Eq.(15), ω_j is the natural frequency of order "*j*", $k_j=(2j-1)\pi/2L$ and μ is the linear density of the material of the bar.

The weak formulation is derived by the used of the Galerkin procedure and can be stated as: Find $\tilde{\boldsymbol{u}}(x,t)\in Kin_t$ such that:

$$EA\int_0^L\frac{\partial\tilde{\boldsymbol{u}}}{\partial x}\frac{\partial\boldsymbol{v}}{\partial x}dx+\frac{EA}{c^2}\int_0^L\frac{\partial^2\tilde{\boldsymbol{u}}}{\partial t^2}dx=\int_0^L q\boldsymbol{v}dx+\Im(t)\boldsymbol{v},\quad \forall\boldsymbol{v}\in Var_t \tag{16}$$

The sets Kin_t and Var_t are defined by:

$$Kin_t=\left\{\tilde{\boldsymbol{u}}\in H^1(\Sigma)/\,\tilde{\boldsymbol{u}}=0,x=0,t\in[0,T]\right\}\ \text{ and }\ Var_t=\left\{\boldsymbol{v}\in H^1(\Sigma)/\,\boldsymbol{v}=0,x=0,t\in[0,T]\right\} \tag{17}$$

The semi-discrete formulation of the problem is obtained by the use of

$$\boldsymbol{u}_h(x,t)=\mathbf{N}(x)\boldsymbol{U}(t)\ \text{ and }\ \boldsymbol{v}_h(x,t)=\mathbf{N}(x)\boldsymbol{V}(t) \tag{18}$$

where $\mathbf{N}(x)$ is the matrix of approximation functions defined on Eq.(12), which depends only on the position variable "*x*" and $\boldsymbol{U}(t)$ and $\boldsymbol{V}(t)$ are the vectors of nodal values of displacements, which are function of time "*t*". $\boldsymbol{U}(t)$ and $\boldsymbol{V}(t)$ are

$$\boldsymbol{U}^T(t)=\left[u_1^1(t)\quad u_2^1(t)\quad\cdots\quad u_i^\alpha(t)\quad\cdots\quad u_p^n(t)\right]\ \text{ and }\ \boldsymbol{V}^T(t)=\left[v_1^1(t)\quad v_2^1(t)\quad\cdots\quad v_i^\alpha(t)\quad\cdots\quad v_p^n(t)\right] \tag{19}$$

with $\alpha=1,...,n;\ \ i=1,...,p.$ The matrix $\mathbf{B}$ used in the propagation problem is defined by Eq.(12). The semi-discrete form that corresponds to Eq.(16) is now

$$\int_0^L\mathbf{B}^T EA\mathbf{B}dx\boldsymbol{U}(t)+\int_0^L\mu\mathbf{N}^T\mathbf{N}dx\ddot{\boldsymbol{U}}(t)=\mathbf{N}^T\Im(t)+\int_0^L\mathbf{N}^T q(t)dx\,. \tag{20}$$

The Eq.(20) can be written in its compact form as

$$\mathbf{K}\boldsymbol{U}(t)+\mathbf{M}\ddot{\boldsymbol{U}}(t)=\boldsymbol{F}(t) \tag{21}$$

where

$$\mathbf{K}=\int_0^L\mathbf{B}^T EA\mathbf{B}dx\ \text{ and }\ \mathbf{M}=\int_0^L\mu\mathbf{N}^T\mathbf{N}dx \tag{22}$$

and

$$\boldsymbol{F}(t)=\mathbf{N}^T\Im(t)+\int_0^L\mathbf{N}^T q(t)dx\,. \tag{23}$$

3.2.1. Propagation results

The phenomenon of propagation in a rod is studied by means of the wave front effects in the displacement field. The essential boundary conditions state that the displacement and the velocity fields are zero on the clamped end and an impulsive force, natural boundary condition, is applied in the free edge. The impulsive force is

$$F(t)=\begin{cases}10^6 N, & t<3\times10^3\Delta t\\ 0, & t>3\times10^3\Delta t\end{cases}. \tag{24}$$

A time increment value of $\Delta t = 3,448073\times10^{-8}\,s$ was used in the numerical examples for the direct integration. It was chosen based on the following estimative: $\Delta t = {T_n}/{20}$, where $T_n = {1}/{\omega_n}$ and ω_n is the higher natural frequency, see Bathe (1996). The numerical results are obtained in time domain based on the direct integration using the Newmark's implicit integration method. The numerical results consists of the wave front profile in terms of the displacement field at the instant $T = 10^4\Delta t$. The results shown in Figs. 5 and 6 are related to the following cases:

- Case A: FEM approximation space with regularity $C^0(\Sigma)$ with 50 linear elements and 50 dof.
- Case B: GFEM approximation space with regularity $C^0(\Sigma)$ with 25 particles enriched with $p=1$ order.
- Case C: GFEM approximation space with regularity $C^2(\Sigma)$ with 25 particles enriched with $p=1$ order.

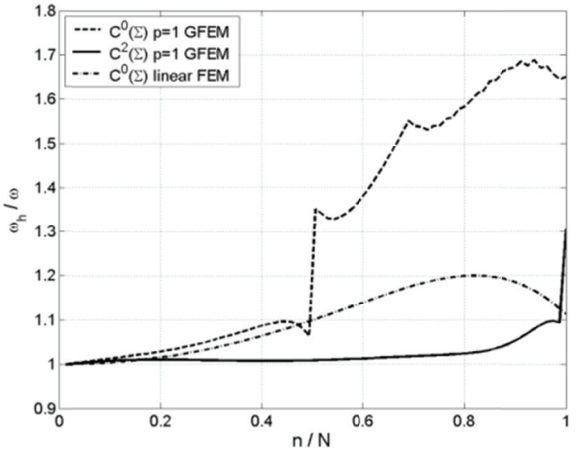

Figure 5 – Normalized natural frequencies values for the rod wave propagation problem.

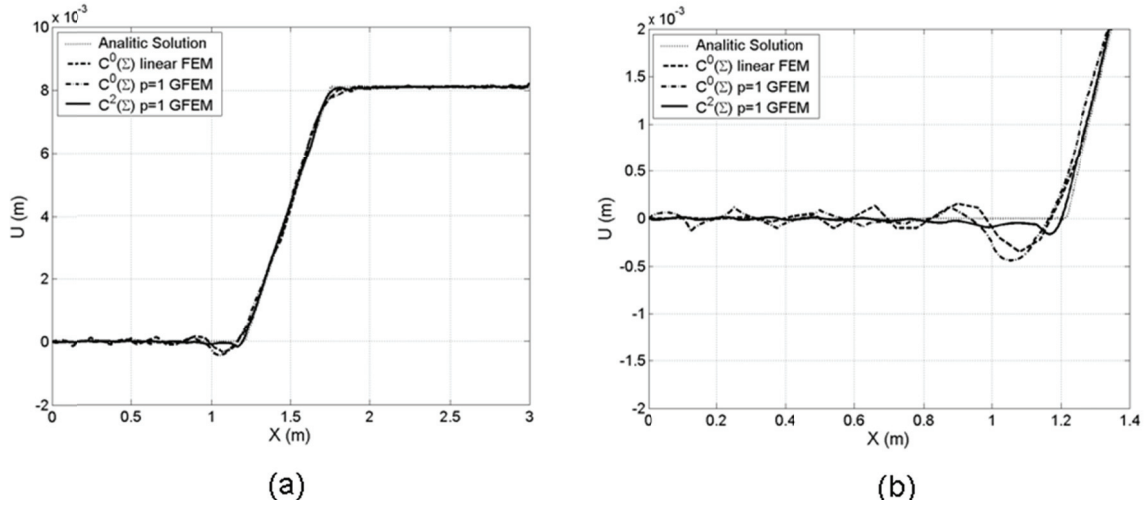

Figure 6 – Comparison between analytical and numerical solution for the displacement field $U(x,t)$ at the instant $10^4\Delta t$. a) Global solution; b) detail at the region of the large oscillation.

Figure 6 shows the results achieved for the predicted natural frequencies for the three cases mentioned above. For Case A, the behavior is smooth but not precise. For the Case B, it is noted the arising of spurious frequencies for values of frequencies greater than 0.5 in the normalized spectra. On the other hand, the results achieved for the Case C presents a smooth and more precise numerical prediction for practically all normalized spectra. The observed results

clearly demonstrate a decrease in the error when the regularity of the GFEM approximation space is augmented, which agrees with the conclusions drawn by the analysis of the error estimator in Eq. (1) but for the FEM. It seems to follow the same behavior.

The results achieved for the wave front are depicted in Fig. 6. Figure 6(a) shows the wave front displacement numerical results for the same three Cases previously mentioned. The numerical results are confronted with the analytical wave front displacement solution. Figure 6(b) shows a zooming at zone of large numerical result oscillation. Again, the better result is achieved for the Case C, where we clear note the influence of the $C^2(\Sigma)$ approximation space. The explanation for such improved solution is closely related to the improved solution of the eigenmodes depicted in Fig.3. It is known that the wave propagation originated by impulsive forces in solid media excite an elevated number of high frequencies and therefore natural frequencies. The better is the numerical prediction of high eigenmodes the better the numerical capture of the wave front displacement.

3.3. Free vibrations in axisymmetric plates and shells

In this work, axisymmetric plates and shells are modelled by the degenerated solid element proposed by Ahmad (1970), together with the axisymmetric constraint described by Hughes (1987). According to this constraint, the medium surface of the element is represented by a medium plane curve containing a certain number of nodes. The number of nodes depends on the type of element used. Here we use the quadratic element, called Q3 in the text. A full description of the degenerated element can be found in Garcia and Proença (2007).

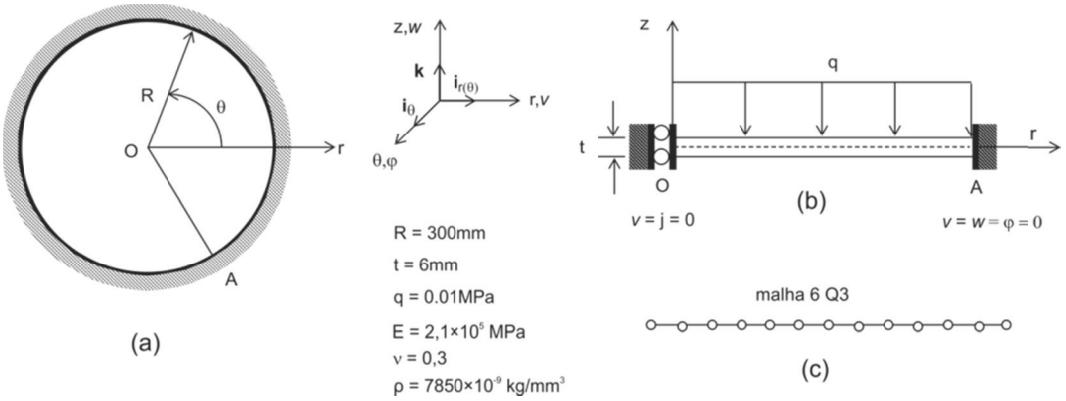

Figure 7 - Circular thick plate model. (a) Circular plate with clamped boundary; (b) Model problem and boundary conditions; (c) Mesh.

3.3.1. Locking effects in the first natural frequency

Shear locking in plates and shells is a characteristic problem that arises when the first order kinematic theory (Reissner-Mindlin) is employed and the approximation space is unable to meet the requirement of zero shear deformation when the thickness goes to zero. In static problems, this numerical phenomenon is manifested by a significant increase in stiffness when the thickness goes to zero. However, in free-vibration problems, this phenomena is evidenced by an unexpectedly increase in the first natural frequency.

The following results correspond to the numerical study of a circular plate with geometry, boundary conditions and material properties as indicated in Fig. 7. Here, we vary the thickness *t*. The discretisation strategies consider 304 dof for the FEM and 310 dof for the GFEM. The influence of the approximating space in circumvents the shear locking is analysed. So, for a known regularity and number of dof, we increase the polynomial order of the approximation space. The characteristics of the discretisation and approximation space are:

i. FEM – $C^0(\Sigma)$ – 50 quadratic elements;

ii. FEM – $C^0(\Sigma)$ – 26 quartic elements;

iii. GFEM – $C^0(\Sigma)$ – 35 active nodes – $p = 2$;

iv. GFEM – $C^0(\Sigma)$ – 20 active nodes – $p = 4$;

v. GFEM – $C^2(\Sigma)$ – 35 active nodes – $p = 2$;

vi. GFEM – $C^2(\Sigma)$ – 20 active nodes – $p = 4$.

The results are presented in Fig. 8. The results are given in terms of the normalised natural frequency, in which ω_h is the numerical frequency and ω is the analytical solution for thin plate free-vibration, see Soedel (2005), versus the ratio *R/t*, in which *R* is the radius and *t* is the thickness of the plate. The choice of the first frequency, for the analysis of

shear locking, remains in association with the static bending mode problem under a uniformly distributed load on the plate surface.

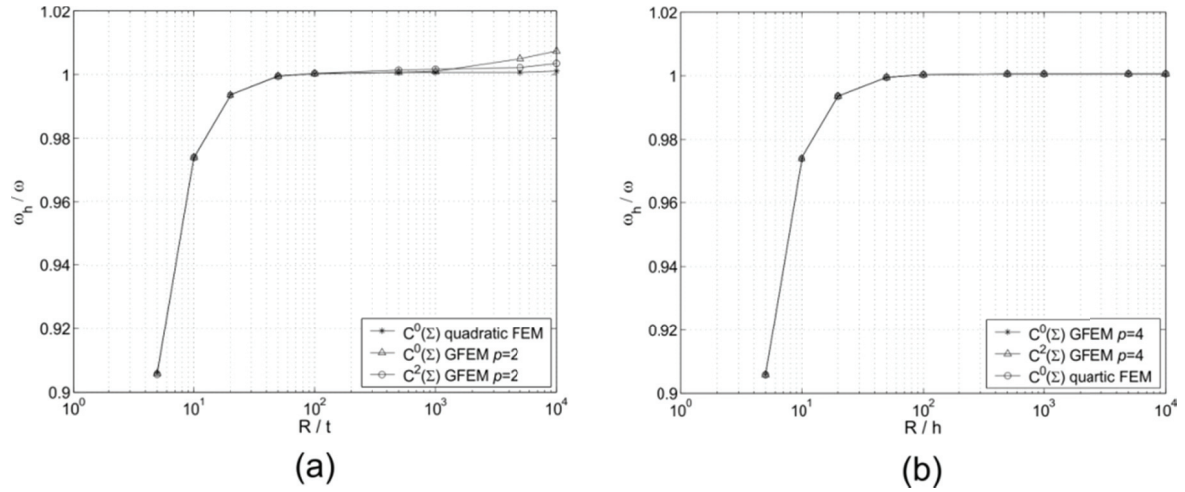

Figure 8 – Plate bending mode results. (a) Convergence results for quadratic approximation spaces; (b) Convergence results for quartic approximation spaces.

Figure 8(a) presents the results for quadratic approximation spaces. Notice that for $R/t > 10^3$, strategies *ii* and *iii* lose convergence, showing a deviation from the analytical solution. This deviation is clearly more severe for the $C^0(\Sigma)$ approximation space. On the other hand, for the FEM result, there is no sign of the locking effect. Figure 8(b) shows the predicted values for the quartic approximation spaces. There is no sign of shear locking in these results, neither for the FEM nor for GFEM. When a comparison is established among the results for cases *iii* and *iv*, in relation to the results for cases *v* and *vi*, we clearly note that the increase in the polynomial is more efficient than increase in the approximation space regularity.

3.3.2. Intermediate high natural frequencies in a Spherical Cap

The results presented in this section correspond to determination of the natural frequencies of a spherical cap, depicted in Fig. 9.

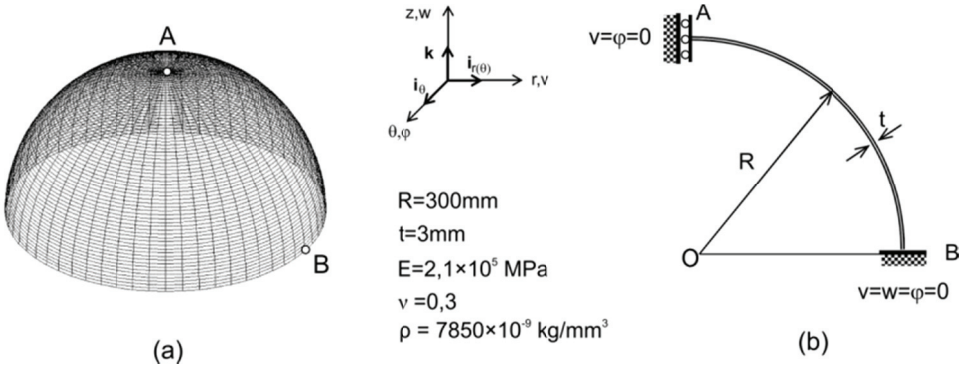

Figure 9 - Shell model: a) Spherical cap; b) Axisymmetric model with geometric, material parameters and boundary conditions.

Table 1 - $\Omega_i = \omega_h^i / \omega_r^i$ for the spherical cap.

Case	P	NDOF	Ω_1	Ω_{10}	Ω_{20}	Ω_{30}	Ω_{40}
i	2	304	1.0002	1.0013	1.0259	1.0620	1.1136
iii	2	301	1.0000	1.0026	1.0560	1.0390	1.2028
v	2	301	1.0004	1.0076	1.0720	1.0360	1.0387

Here, we are also interested in evaluating the influence of the regularity of the approximation space in capturing axisymmetric natural frequencies. Now, the objective of the analysis is to determine intermediate high

frequencies, that is, frequencies greater than 10% of the number of dof estimated by $\left[\mathbf{K}-\omega^2\mathbf{M}\right]\boldsymbol{U}=\mathbf{0}$. The results are compared with a reference solution, which is given by the "rule of thumb", see Givoli (2007). The spherical cap model is depicted in Fig. 9, where the geometry, material and boundary conditions are shown. The results are in terms of the normalised natural frequency obtained from strategies *i*, *iii* and *v*, relative to the reference solution. Here, a constant thickness of $t = 3$ *mm* is assumed. In this analysis, 52 (602 dof) quadratic axisymmetric elements were uniformly distributed for the reference solution. The number of eigenvalues, *M,* that can be obtained with an error, $\varepsilon = 0.001$, predicted by the reference solution, "rule of thumb", is $M = 106$. The results for the selected strategies are presented in Table 1.

The subscript "*i*" in Ω_i in Table 1 indicates the number of the mode associated with the natural frequency and "*p*" is the order of the approximation space. Notice that up to the mode number 10, the results are precise for all strategies. However, after this value, the results begin to suffer monotonic deviations in strategy *i* and oscillatory behaviour in strategy *iii*. On the other hand, in contrast to the other strategies, the results for strategy *v* show lower error for modes greater than 20.

4. CONCLUSION

In this work, an approximation space generated by a proposed GFEM is used in numerical solving problems of free vibrations and wave propagations in elastic media. The proposed GFEM is based on a particular class of weight functions, which assures regularity C^k, *k* even, and were enriched using monomials up to a desired order *p*. Special attention is given for axisymmetric plates and shells problems. In general, the results presented in this work show the positive influence of the approximation space regularity on the capturing of free vibration and mechanical wave propagation. In the simple rod problem, it is shown that higher the regularity of the approximation space, higher number of frequencies obtained with accuracy. The results observed in the rod free vibration problem are corroborated by the numerical results achieved for the axisymmetric spherical cap problem. For the plate case, some limitations were observed related to the kinematic model that leads to the occurrence of locking phenomena, which is evidenced in first natural mode. The results clearly show the locking presence when using second order enriched GFEM spaces, however, less severe than in the static problem. They are circumvented by using higher approximation spaces. It is evident the influence of the approximation space regularity on the accuracy of modes greater than 10% of the number of degrees of freedom. Despite not providing results for spaces constructed to approach two or three dimensions problems, it is believed that the results must confirm the results observed in this work. Studies are been conducted to investigate the properties of the proposed approximation space in higher dimensions.

5. ACKNOWLEDGEMENTS

The authors wish to acknowledge the support of the CNPq, Conselho Nacional de Desenvolvimento Científico e Tecnológico of Brazil. Grant numbers 473343/2008-8 and 303662-2009-3.

6. REFERENCES

Bathe, K.J., 1996, "Finite Element Procedures", Prentice Hall, Englewood Cliffs, New Jersey 07632.

Cottrell, J.A., Hughes, T.J.R., Reali, A. and Sangalli, G., 2007a, "Isogeometric discretizations in structural dynamics and wave propagation", ECOMAS Thematic Conference.

Cottrell, J.A., Hughes, T.J.R. and Reali, A., 2007b, " Studies of refinement and continuity in isogeometric structural analysis", Computer methods in applied mechanics, Vol. 196, No. 41-44, pp 4160-4183.

Clough, R.W. and Penzien, J., 2003, "Dynamic of Structures", Computer and Structures, third edition.

Garcia, O.A and Proença, S.P.B., 2007, "Linear analysis of axis-simmetric plates and shells by Generalized Finite Element Method", Latin American Journal of Solid and Structures, Vol. 4, No. 1, pp. 121-148.

Givoli, D., 2007, "On the number of reliable finite-element eigenmodes", Communications in Numerical Methods in Engineering, Vol. 24, No. 12, pp. 1967-1977.

Hughes, T.J.R., 1987, "The Finite Element Method – Linear Static and Dynamic Finite Element Analysis", Dover Publications.

Melenk, J.M. and Babuska, I., 1996, "The partition of unity finite element method: Basic theory and applications", Computer Methods in Applied and Engineering, Vol. 139, No 1-4, pp. 289-314.

Oden, J.T., Duarte, C.A and Zienkiewicz, O.C., 1996, "A new cloud-based hp finite element method", Tec. Rep. TICAM Report 96-55, The University of Texas, Austin, Texas, USA.

Soedel, W., 2005, "Vibrations of shells and plates", third edition, Taylor and Francis e-Library, New York.

7. RESPONSIBILITY NOTICE

The authors are the only responsible for the printed material included in this paper.